Physical and geometric constraints shape the labyrinth-like nasal cavity

David Zwicker[a,b,1], Rodolfo Ostilla-Mónico[a,b], Daniel E. Lieberman[c], and Michael P. Brenner[a,b]

[a]John A. Paulson School of Engineering and Applied Sciences, Harvard University, Cambridge, MA 02138; [b]Kavli Institute for Bionano Science and Technology, Harvard University, Cambridge, MA 02138; and [c]Department of Human Evolutionary Biology, Harvard University, Cambridge, MA 02138

Edited by Leslie Greengard, New York University, New York, NY, and approved January 26, 2018 (received for review August 29, 2017)

The nasal cavity is a vital component of the respiratory system that heats and humidifies inhaled air in all vertebrates. Despite this common function, the shapes of nasal cavities vary widely across animals. To understand this variability, we here connect nasal geometry to its function by theoretically studying the airflow and the associated scalar exchange that describes heating and humidification. We find that optimal geometries, which have minimal resistance for a given exchange efficiency, have a constant gap width between their side walls, while their overall shape can adhere to the geometric constraints imposed by the head. Our theory explains the geometric variations of natural nasal cavities quantitatively, and we hypothesize that the trade-off between high exchange efficiency and low resistance to airflow is the main driving force shaping the nasal cavity. Our model further explains why humans, whose nasal cavities evolved to be smaller than expected for their size, become obligate oral breathers in aerobically challenging situations.

respiration | fluid dynamics | scalar transport | evolution

The nose not only allows us to smell but also humidifies, heats, and cleans inhaled air before it reaches the lungs. All these vital tasks depend critically on nasal airflow, which is driven by the pressure difference created by the lungs and depends on the complex geometry of the nasal cavity. Nasal geometries vary considerably among vertebrates in general (1) and among mammals in particular (2–4), ranging from the complex labyrinth-like internal nasal cavity of dogs to the unique structure of humans that combines relatively simple geometry in a short internal nasal cavity with an additional external nasal vestibule; see Fig. 1. These qualitative differences in nasal geometry were likely selected as adaptations to different functional requirements, but how the geometry of the nose influences the airflow and thus the function of the nose is a long-standing unsolved problem.

The nasal cavity is a complex, air-filled space that connects the two nostrils with the throat; see Fig. 1*A*. All mammals have an internal nasal cavity, but humans are unique in having an additional external vestibule with inferiorly oriented nostrils (5). The two sides of the cavity are separated by the nasal septum and merge only behind the posterior nasal cavity (choanae) that separates the nasal cavity from the pharynx. Each side can be further divided into the main pathway (turbinates) and large side chambers (sinuses). The walls of the nasal cavity are covered by a highly vascularized bed of epithelial tissue overlain by a 10-μm-thick layer of mucus, which is slowly propelled backward by cilia (6). The mucus consists mainly of water and thus humidifies inhaled air. Additionally, the nasal epithelium warms the air and absorbs airborne particles, like odorants.

We here study how the geometry of the nasal cavity influences the airflow and the associated processes of heating and humidifying the inhaled air. Generally, we expect that a narrower geometry improves the efficiency of heating and humidification at the expense of greater resistance to airflow. Since this trade-off likely plays an important role in shaping nasal cavities, we determine the shape that has the lowest resistance to airflow for a given conditioning of the inhaled air. Here, we have to take into account geometric constraints imposed by the shape of the head that determine the length of the nasal cavity, its cross-sectional area, and, generally, the shape of the space that it occupies. To tackle this complex problem, we first show that, without geometric constraints, optimal shapes have slender cross-sections. We then demonstrate that these shapes can be compacted into the typical labyrinth-like shapes without much loss in performance.

Results

The Flow in the Nasal Cavity Is Laminar. It has been suggested that the flow in the nasal cavity is turbulent (7, 8), since the speeds are high and nasal geometry is complex. Indeed, turbulence can easily be induced in the surrounding air by exhaling heavily, as is apparent on a cold winter day. Inside the nose, turbulent flow would induce additional mixing that improves the heating and humidification of the inhaled air (9), but it also implies a larger resistance to flow. It is thus unclear whether turbulence would be beneficial.

To see whether turbulence occurs inside the nasal cavities of animals of various sizes, we first estimate the mean speed $\bar{u}$ using experimentally determined scaling relations of respiratory quantities with body mass; see Table 1. In particular, we combine the volumetric flux Q, the volume V of the nasal cavity, and the length of the skull as a proxy for the length L of the cavity, to obtain $\bar{u} = QL/V \approx 0.3\ \mathrm{m/s} \cdot (M/\mathrm{kg})^{0.15 \pm 0.06}$. Since $\bar{u}$ is much smaller than the speed of sound, the flow is incompressible. For the flow to be turbulent, inertia has to dominate viscous dampening. The ratio of these two effects is quantified by the Reynolds

Significance

Although nasal cavities fulfill similar tasks across animals, their geometry varies widely. One such task is heating and humidifying the inhaled air, which works best if the nasal cavity is narrow. However, narrow geometries have a large resistance to flow. We show that these opposing geometrical requirements are critical for shaping the nasal cavity and strongly restrict the local gap width. In contrast, the overall shape has little influence on the resistance and air conditioning, so the observed labyrinth-like patterns could emerge from geometric constraints imposed by the head. Our theory predicts geometric parameters of nasal cavities quantitatively, and it suggests that the surprisingly small nasal cavities of humans force us to become oral breathers during heavy exercise.

Author contributions: D.Z., R.O.-M., D.E.L., and M.P.B. designed research, performed research, analyzed data, and wrote the paper.

The authors declare no conflict of interest.

This article is a PNAS Direct Submission.

[1]To whom correspondence should be addressed. Email: david.zwicker@ds.mpg.de.

This article contains supporting information online at www.pnas.org/lookup/suppl/doi:10.1073/pnas.1714795115/-/DCSupplemental.

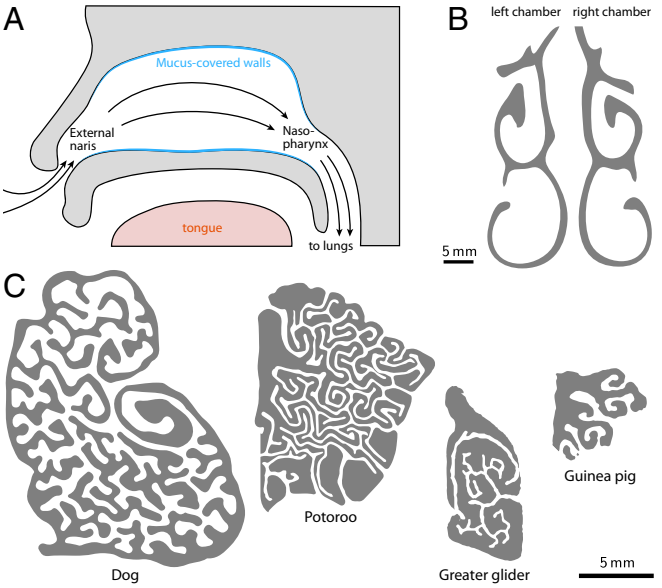

Fig. 1. Schematic cross-sections of nasal cavities. (*A*) Sagittal cross-section showing how air flows though the nasal cavity during inhalation. (*B*) Coronal cross-section of a human nasal cavity showing the complex shape of the two air-filled nasal chambers (gray region). The airflow is perpendicular to the plane. (*C*) Coronal cross-sections of the right nasal chambers of mammals (sorted from left to right by decreasing body weight): *Canis lupus familiaris* (dog) (14), *Potorous tridactylus* (long-nosed potoroo) (3), *Petauroides volans* (greater glider) (3), and *Cavia porcellus* (guinea pig) (31). Reprinted with permission from ref. 14 (dog), ref. 3 (potoroo and greater glider), and ref. 31 (guinea pig). (Scale bars in *B* and *C*, 5 mm.)

number $Re = \bar{u} R_\mathrm{h}/\nu$, where $\nu \approx 1.5 \cdot 10^{-5}$ m^2/s is the kinematic viscosity of air (10) and R_h is the characteristic linear dimension of the flow. In complex geometries, R_h is given by the hydraulic radius $R_\mathrm{h} = 2V/S$, where V and S are the volume and surface area of the geometry, respectively. Using the scalings given in Table 1, we find $Re = 2LQ/(\nu S) \approx 70 \cdot (M/\mathrm{kg})^{0.36 \pm 0.06}$, so *Re* increases with body mass. Typically, flows are turbulent when *Re* is about 10^3, with the precise transition depending weakly on the flow geometry; for example, flow between parallel plates (11) is turbulent at a lower *Re* than in pipes (12). Regardless, this indicates that turbulence occurs only in animals heavier than about 10^3 kg. Indeed, numerical simulations have shown that the narrow geometry of the nasal cavity prevents the development of turbulence in humans (13), dogs (14), and rats (15).

Another ubiquitous feature of nasal airflow is the oscillatory motion caused by natural breathing, which generally induces additional resistance and also limits the humidification and heating of the air. However, this is only important when the characteristic length R_h is smaller than the length $(\nu/f)^{1/2}$ associated with the frequency f of the flow (16). Using the scalings from Table 1, we find $R_\mathrm{h}(f/\nu)^{1/2} \approx 0.7 \cdot (M/\mathrm{kg})^{0.09 \pm 0.07}$, which depends only weakly on the body mass M, so the effect of pulsatility is similar for all animals. We show in *SI Appendix* that the resistance increases by about 50 % compared with steady flow, since R_h is comparable to $(f/\nu)^{1/2}$. Note that, if the frequency f were much higher, the resistance would increase strongly, while a lower frequency would imply a larger tidal volume and thus require a larger lung. The associated trade-off might set the respiratory rate, but, since the pulsatility affects all animals similarly, we can simply analyze steady flow here.

The Optimal Nasal Cavity Has a Uniform Gap Width. We seek the geometry of the nasal cavity with the lowest resistance to airflow for a given efficiency of heating and humidifying the air under the constraint of a given volumetric flux, length, and cross-sectional area. We thus need to calculate the dependence of the airflow and its physical properties on the geometry of the nasal cavity. Since nasal cavities are typically straight, we first focus on varying the cross-sectional shape.

The flow through the cavity is driven by a pressure difference P generated by the lungs. Since the flow in a straight nasal cavity is laminar, stationary, and incompressible, the velocity field only has a component u in the axial direction, which obeys the Poisson equation

$$\boldsymbol{\nabla}_\perp^2 u(x,y) = -\frac{P}{\eta L}, \qquad [1]$$

with $u = 0$ at the walls (*SI Appendix*). Here, $\boldsymbol{\nabla}_\perp^2$ denotes the Laplacian in the cross-sectional plane, L is the length of the cavity, and $\eta \approx 1.8 \cdot 10^{-5}$ Pa.s is the dynamic viscosity of air (10). Solving Eq. **1** for u, we obtain the volumetric flux $Q = \int u \, \mathrm{d}x\mathrm{d}y$, which scales with P. The resistance $K = P/Q$ is then independent of Q and can be expressed as

$$K = C_K \cdot \frac{\eta L}{A^2}, \qquad [2]$$

where C_K is a nondimensional parameter that depends only on the cross-sectional shape; see *SI Appendix*. We can thus quantify the influence of the cross-sectional shape on the airflow by simply studying its effect on C_K.

The heating and humidification properties of the nasal cavity can be quantified by the change in temperature and concentration of water vapor in the air after it flowed through the cavity. Both quantities can be described as a passive scalar c that is transported with the flow, diffuses, and is exchanged with the walls of the cavity. In a stationary state, the scalar c thus obeys

$$0 = D\boldsymbol{\nabla}^2 c - \partial_z(uc), \qquad [3]$$

where D denotes the diffusivity, and boundary conditions are imposed by the epithelial tissue. For simplicity, we first consider the case where the boundary is kept at body temperature and maximal humidity, which implies a constant scalar value c_b at the walls. While flowing through the cavity, the cross-sectionally averaged scalar $\bar{c}(z)$ will thus change from its ambient value $\bar{c}(0) = c_\mathrm{a}$ to approach c_b. The extent of this process at the end of the cavity is quantified by the scalar exchange efficiency

$$\mathcal{E} = \ln\left(\frac{\bar{c}(0) - c_\mathrm{b}}{\bar{c}(L) - c_\mathrm{b}}\right), \qquad [4]$$

which is larger the closer $\bar{c}(L)$ gets to c_b. We show in *SI Appendix* that $\bar{c}(z)$ can be expressed as $\bar{c}(z) = c_\mathrm{b} + \sum_n a_n e^{-z/\lambda_n}$, where λ_n are length scales that follow from the generalized eigenvalue problem

Table 1. Scaling of respiratory quantities *y* with body mass *M* given in units of kilograms, $y = a(M/\mathrm{kg})^b$

Quantity *y*	Prefactor *a*	Exponent *b*	Source
Skull length *L*	7 cm	0.32 ± 0.01	(18)
Surface area *S*	19 cm^2	0.74 ± 0.03	(18)
Nasal volume *V*	2.9 cm^3	0.96 ± 0.03	(18)
Tidal volume V_t	7.7 cm^3	1.04 ± 0.01	(33)
Respiratory rate *f*	0.89 s^{-1}	-0.26 ± 0.01	(33)
Cross-section *A*	0.4 cm^2	0.63 ± 0.04	$A = V/L$
Volumetric flux *Q*	14 cm^3/s	0.78 ± 0.02	$Q = 2V_\mathrm{t}f$

$$-D\nabla_{\perp}^2 c_n(x,y) = \lambda_n^{-1} u(x,y) c_n(x,y), \quad [5]$$

and the coefficients a_n can be determined from the initial value $\bar{c}(0)$ at the inlet. Note that we here neglected the small axial diffusion term, since it is dominated by advection ($\bar{u}L \gg D$). Moreover, in the simple case of a long cavity, entrance effects can be neglected, and only the mode with the largest λ_n contributes to $\mathcal{E}$. In this case, we have

$$\mathcal{E} = C_{\mathcal{E}} \cdot \frac{DL}{Q}, \quad [6]$$

where $C_{\mathcal{E}} = Q/(\lambda_1 D)$ is a nondimensional factor associated with the largest λ_n. We show in *SI Appendix* that $C_{\mathcal{E}}$ depends only on the cross-sectional shape and captures how the shape affects the scalar exchange.

To find the geometry that has minimal resistance K for a given exchange efficiency $\mathcal{E}$, we determine the respective prefactors C_K and $C_{\mathcal{E}}$ for several simple shapes; see Fig. 2. C_K is lowest for a circular shape, but the associated $C_{\mathcal{E}}$ is also minimal. As expected, both C_K and $C_{\mathcal{E}}$ increase when shapes become narrower for larger aspect ratios, which illustrates the trade-off between low resistance and large exchange efficiency. In fact, for all shapes considered, the ratio $C_K/C_{\mathcal{E}}$ approaches a constant for large aspect ratios, indicating that both quantities increase proportionally. However, not all shapes perform similarly: The resistance of rectangular shapes is up to 40% lower than that of ellipses with the same exchange efficiency.

To understand what geometric features lead to good performance, we numerically determine how shapes need to be altered to lower the resistance at constant exchange efficiency; see Fig. 3 and *SI Appendix* for details. This sensitivity analysis suggests that sharp corners and narrow regions are detrimental, as indicated by the large arrows in Fig. 3. However, it does not show clearly why rectangular shapes outperform ellipses. To understand this aspect better, we use the sensitivity analysis to obtain optimal shapes by iterative adaptation as described in *SI Appendix*. Fig. 3

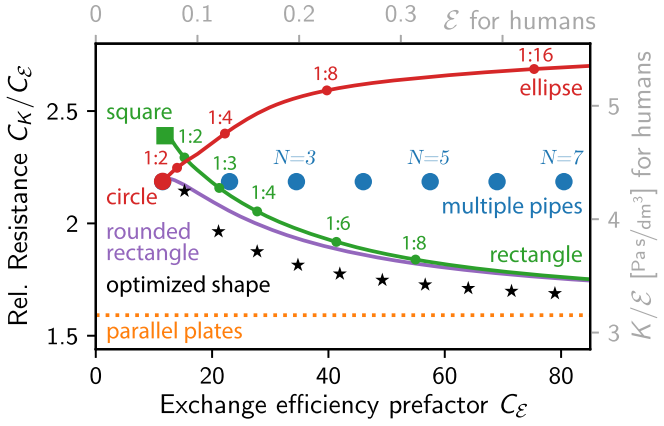

Fig. 2. Comparison of the relative resistance $K/\mathcal{E}$ for different cross-sectional shapes as a function of a prescribed exchange efficiency $\mathcal{E}$. Only the prefactors C_K and $C_{\mathcal{E}}$ are shown, but the top and right axes display the respective values for human noses with parameters given in Table 2. The considered shapes are a circular pipe (large red circle), a square duct (green square), elliptical ducts (red line, ratio of half-axes indicated at support points), rectangular ducts (green line, ratio of sides indicated at support points), rectangular ducts with rounded corners (violet line), *N* circular pipes in parallel (blue dots), and numerically optimized shapes (black stars). The resistance of the proper cross-sections is bounded by the value for parallel plates (orange dotted line). Solid lines are quadratic interpolations between the support points (dots) where values were calculated numerically and cross-checked with the literature (32).

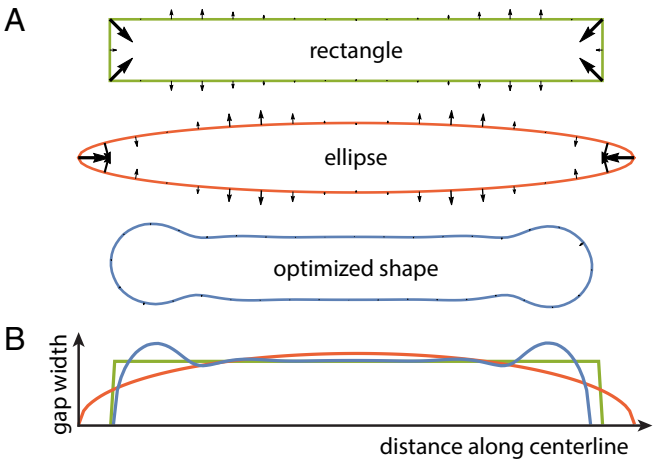

Fig. 3. (*A*) Sensitivity to shape perturbations of three cross-sectional shapes. The arrows indicate the magnitude of the decrease of the resistance prefactor C_K (arrow length) when the shape is locally perturbed in the normal direction (arrow direction) at fixed area *A* and scalar exchange efficiency $C_{\mathcal{E}}$; see *SI Appendix* for numerical details. (*B*) Width perpendicular to the centerline as a function of position for the three shapes shown in *A*. This gap width is uniform in the midsection of optimal shapes and rectangles, while it varies significantly in ellipses.

and *SI Appendix*, Fig. S2 show that optimal cross-sections are dumbbell-shaped, with a slender midsection. We compare the midsections of different shapes by quantifying the width of the shape perpendicular to the centerline as a function of the distance along the centerline. Fig. 3 shows that this gap width is uniform for the optimal and rectangular shapes, while it varies significantly for the ellipse. Taken together, optimal shapes are thus rounded and posses a uniform gap width.

The optimal width of the gap can be estimated from the asymptotic geometry of two parallel plates, which provides a lower bound for the achievable resistance; see Fig. 2. This geometry corresponds to a rectangular duct with the two small sides replaced by unphysical periodic boundary conditions, so the cross-sectional area A is still well defined. The prefactor for the scalar exchange in this geometry is $C_{\mathcal{E}} = 7.54\, A\ell^{-2}$, where ℓ is the plate separation. Using Eq. **6**, we can then solve for the ℓ that results in a given scalar exchange efficiency $\mathcal{E}$,

$$\ell = 2.75\sqrt{\frac{D\tau}{\mathcal{E}}}, \quad [7]$$

where $\tau = LA/Q$ is the time it takes air to cross the cavity. The gap width must thus be similar to the typical distance $(D\tau)^{1/2}$ the scalar diffuses while passing through the cavity (17).

The result of our theoretical considerations is twofold: First, we qualitatively predict that natural selection favors nasal cavities where the separation between the walls is approximately constant everywhere. Second, we quantitatively predict the optimal gap width, either from the aspect ratio of realistic ducts that lead to a given $\mathcal{E}$ or by using Eq. **7** as an approximation.

The Theory Agrees with Experimental Measurements. Nasal cavities described in the literature are typically narrow and exhibit little variation in gap width (2, 3), which agrees with our theory qualitatively. For a quantitative comparison, we consider geometric measurements of nasal cavities of canid and arctoid carnivorans that have been reconstructed in silico from CT scans (18). The associated scalings of the geometric parameters with body mass are summarized in Table 1. The volumes V of the cavities and the lengths of the skulls scale isometrically, but the surface

areas of the cavities exhibit significant positive allometry; that is, in heavier animals, it is larger than expected from geometric scaling.

To test whether our theory can explain the observed data, we calculate the surface area of the optimal geometry of the nasal cavity as a function of the constrained parameters D, A, L, Q, and $\mathcal{E}$. Here, D is the scalar diffusivity, which is either the mass diffusivity of water vapor, $D_{\mathrm{w}} = 2.5 \cdot 10^{-5}\ \mathrm{m}^2/\mathrm{s}$ (10), or the diffusivity of heat at room temperature, $D_{\mathrm{h}} = 2.2 \cdot 10^{-5}\ \mathrm{m}^2/\mathrm{s}$ (19). Since both values are similar, we just consider the slower diffusivity, $D = D_{\mathrm{h}}$, implying that humidification of the air will be slightly better than its heating. The other parameters could be different for each animal, but, since they have not been measured independently in all animals, we use reported scaling relations with body mass for A, L, and Q; see Table 1. Finally, we consider the scalar exchange efficiency $\mathcal{E} = 1$ independent of body mass, implying that temperature and humidity equilibrate with the walls to about 60% in all animals. Indeed, inhaled air is typically heated to about 65% of body temperature (20), and the relative humidity is raised to about 80% (21) in humans.

We first predict the surface area S in the simple geometry of parallel plates, where we can calculate the optimal gap width ℓ explicitly using Eq. **7**. Using the scalings described above, we find $\ell \approx 6\ \mathrm{mm} \cdot (M/\mathrm{kg})^{0.09 \pm 0.04}$. The associated surface area is $S \approx 2V/\ell$, and thus scales as $S \approx 9.8\ \mathrm{cm}^2 \cdot (M/\mathrm{kg})^{0.87 \pm 0.07}$. Fig. 4*A* shows that this predicted scaling agrees well with the measured data. Consequently, our simple scaling theory correctly predicts important geometric properties of real nasal cavities. In particular, the positive allometry of the surface area, which is observed in a wide range of animals (5, 22), is a direct consequence of the negative allometry of the optimal gap width ℓ. Note that, if the gap width scaled isometrically (with $M^{1/3}$), the scalar exchange efficiency $\mathcal{E}$ would drop significantly in larger animals, because it scales as $\mathcal{E} \approx \ell^{-2}$. Taken together, our theory shows that the allometric scaling of geometric parameters of the nasal cavity is a consequence of the physics of the airflow and the scalar exchange.

So far, we considered the idealized geometry of parallel plates, which contains unphysical periodic boundary conditions. For large aspect ratios, this is a good approximation of the more realistic shape of a rectangular duct, but we showed above that the gap width does not scale isometrically and the aspect ratio thus varies with body mass. In particular, smaller animals will have aspect ratios closer to unity, and the scalings derived from the parallel plate model are not accurate in this case; see Fig. 4*A*. To correct this, we numerically determine the rectangular shape with a given cross-sectional area A that leads to the exchange efficiency $\mathcal{E} = 1$. The light-green line in Fig. 4*A* shows the associated surface area as a function of body mass, which now cannot be expressed as a simple scaling law. Note that this correction is insignificant for large animals, which confirms that they have nasal cavities with high aspect ratio where the parallel plates model is accurate. Conversely, there are large deviations for small animals, where the side walls contribute to the surface area significantly. In fact, we find that the exchange efficiency exceeds 1 for small animals even in the case of a square geometry (dashed line in Fig. 4*A*). This high efficiency in small geometries thus suggests that the nasal cavities of small animals have simpler cross-sections, which has, indeed, been observed (2, 3).

Strikingly, one point that deviates strongly from the theoretical prediction in Fig. 4*A* is for humans. The surface area of their nasal cavity is about half of what the scaling suggests, and the volume is even only about 10% of the prediction (Fig. 4*A*, *Inset*). The data point for humans was calculated from a standardized nasal cavity, which was obtained by averaging reconstructed geometries of 30 humans (23), together with typical respiratory parameters given in Table 2. To examine the geometry of human nasal cavities more closely, we compute the local gap width in the standardized nasal cavity using the shape diameter function, which gives the average distance of nearby walls at every point of the surface (24) (Fig. 4*B*), and the hydraulic radius $R_{\mathrm{h}} = 2A/\Gamma$ from the cross-sectional area A and the perimeter Γ (Fig. 4*C*). Both quantifications indicate that the gap width is remarkably constant over a large fraction of the standardized nasal cavity, while the cross-sectional area varies significantly (Fig. 4*C*, *Inset*). However, the measured R_{h} is significantly smaller than the predicted optimal gap width $\ell \approx 3.7$ mm, which follows from Eq. **7** together with the typical respiratory parameters summarized in Table 2. Thus, whereas the geometry of the human nasal cavity agrees with our qualitative result that the gap width should be constant for an efficient scalar exchange, the quantitative prediction deviate significantly from our theory. This is surprising since our theory worked well for all other tested mammals, and this might thus hint at an exceptional behavior of the human nasal cavity. Before we come back to this point in *Discussion*, we next consider how the shape of the head constrains the nasal cavity.

Geometric Constraints Imply Labyrinth-Like Cross-Sections. Natural nasal cavities have a complex labyrinth-like cross-section, which does not resemble the theoretically optimal shape determined above. This difference is likely a consequence of other factors, including additional geometric constraints, since the wide shapes

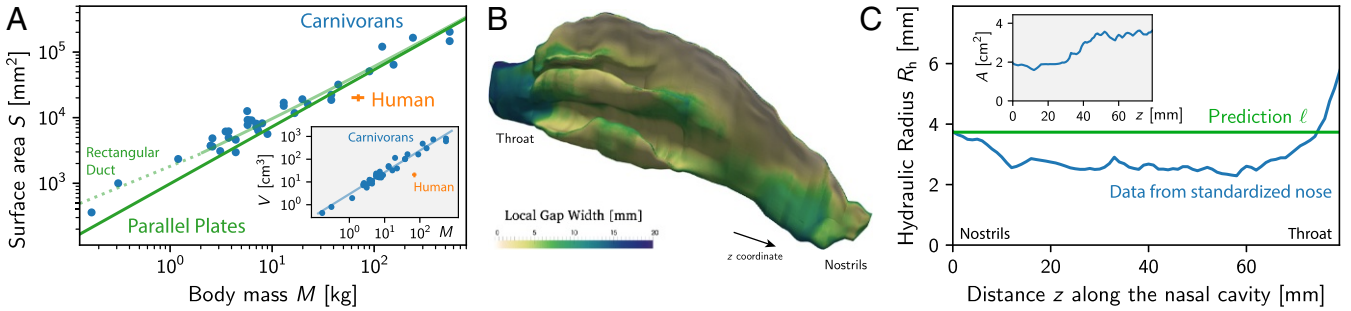

Fig. 4. Comparison of the theoretical predictions to experimental data. (*A*) Surface area *S* of nasal cavities as a function of body mass *M*. Shown are experimentally measured respiratory turbinal surface areas in canid and arctoid carnivorans (18) (blue dots) and in humans (orange cross; bars indicate standard deviation; parameters in Table 2). Our predictions (green lines) follow from the optimal gap width of parallel plates given in Eq. **7** (dark green) and a numerical solution based on a rectangular geometry (light green; dashed part indicates square geometry). Here, we assumed $\mathcal{E} = 1$ and used the scalings given in Table 1. (*Inset*) The associated volumes *V* of the nasal cavities as a function of *M* together with the scaling given in Table 1. (*B*) Local gap width, given by the shape diameter function (24), for the standardized nasal cavity (23). (*C*) Hydraulic radius R_{h} along the main axis *z* of the standardized cavity (23) (blue line) compared with the predicted ℓ given by Eq. **7** (green line), which was calculated for $\mathcal{E} = 1$ and the parameters given in Table 2. (*Inset*) The cross-sectional area *A* of the standardized cavity as a function of *z*.

Table 2. Typical physiological parameters for humans

Quantity	Value	Source
Length of nasal cavity L	(6.5 ± 0.7) cm	(23)
Volume of nasal cavity V	(21 ± 5) cm^3	(23)
Surface area S	(200 ± 25) cm^2	(23)
Cross-sectional area A	(3 ± 1) cm^2	(23)
Tidal volume V_t	(0.5 ± 0.1) L	(34, 35)
Respiratory rate f	(15 ± 4) min^{-1}	(34, 35)
Body mass M	(70 ± 10) kg	(34, 36)
Volumetric flux Q	(15 ± 5) L/min	$Q = 2V_t f$

that we predict would simply not fit into the head. However, the fact that our theory agrees well with experimental data suggests that natural nasal cavities function close to optimally. This would suggest that the bending and branching of the nasal cavity that is necessary to obtain labyrinth-like geometries does not significantly affect the physical principles that led to the optimal gap width given in Eq. **7**. To test this hypothesis, we examine the bending and branching of the cross-section and calculate how it affects the resistance and exchange efficiency. Fig. 5 shows that a U-shaped cross-section has virtually identical properties to a rectangle of the same aspect ratio. Consequently, bending the optimal cross-sectional shape in-plane affects neither the resistance nor the exchange efficiency significantly. To examine the consequence of branching, we consider a T-shaped junction with three rectangular branches of equal length. Numerical simulations indicate that both K and $\mathcal{E}$ are affected more strongly than in the case of bending, but still only change by a few percent compared with an equivalent rectangular shape; see Fig. 5. While the T-shaped junctions can be directly compared with rectangles, they also introduce additional corners, which increase the resistance. We show in *SI Appendix* that optimal junctions are more rounded and impact the resistance less than shown in Fig. 5. Taken together, neither bending nor branching affects the function of the nasal cavity strongly, implying that natural shapes are close to optimal.

Another geometric constraint on the nasal cavity comes from the fact that it must connect the pharynx (and thus the lungs) to the outside world. In humans, this forces a curved flow, which could influence the functions of the nasal cavity (5); see Fig. 1*A*. In general, curved flow increases the resistance and the exchange efficiency significantly (25, 26), but, in the case of the human nose, the bends are localized to the connecting regions, while the main nasal cavity is rather straight. We show in *SI Appendix* that the overall function of the nose is only slightly affected by the bent geometry, consistent with numerical simulations (27). This is because the connecting regions are much wider than the main nasal cavity. Note that this effect is even weaker in animals that have a straighter airflow than humans.

Gradients in the Scalar Exchange Limit Heat and Humidity Loss. Up until now, we have derived the optimal geometry of the nasal cavity by focusing on the efficiency of heating and humidifying the inhaled air. However, improving this efficiency can come at the expense of heat and water loss during exhalation. This is because heating implies that the walls of the nasal cavity are warmer than the inhaled air, while the recapture of heat can only occur when the walls are colder than the exhaled air. Consequently, it is impossible to both heat the air efficiently and recapture most of the heat during exhalation. Such a conflicting requirement also holds for humidification, and we show in *SI Appendix* that small animals would lose about 1% of their body weight due to exhaled water each day. To understand how to prevent this loss while still heating and humidifying inhaled air, the scalar exchange needs to be studied for both inhalation and exhalation.

To study the trade-off between heating the inhaled air and recapturing heat during exhalation, we vary the scalar value c_w that is prescribed at the walls of the nasal cavity. Given that c_w is the same for inhalation and exhalation, we can calculate how the scalar transported with the air changes during these two processes. In particular, we can define a scalar exchange efficiency $\mathcal{E}_{ex}$ for exhalation analogously to $\mathcal{E}_{in}$ for inhalation, given by Eq. **4**. In our calculations above, we considered $c_w = c_b$ and $\mathcal{E}_{in} = 1$, which implies $\mathcal{E}_{ex} = 0$. Heat can be recaptured when c_w is lowered to $c_w = 0.5(c_a + c_b)$, where c_a is the ambient value. A simple analytical model presented in *SI Appendix* shows that, in this case, $\mathcal{E}_{in} = \mathcal{E}_{ex} \approx 0.4$. These values can be improved to $\mathcal{E}_{in} = \mathcal{E}_{ex} \approx 0.5$ when a linear gradient from c_a at the tip of the nose to c_b at the nasopharynx is used. Numerical simulations presented in *SI Appendix* confirm this picture and show that the scalar exchange efficiency is actually higher than predicted by Eq. **6**, because the scalar profile is typically not fully developed and entrance effects matter. Taken together, we conclude that a gradient boundary condition, as observed in nature (28), can improve the recapturing of heat and humidity, at the expense of a lowered exchange efficiency during inhalation. Note that this lower efficiency is approximately compensated by entrance effects that improve the exchange efficiency, so we expect Eq. **7** to work for nasal cavities with gradient boundary conditions and realistic lengths.

Discussion

A critical issue for the shape of the nasal cavity is the opposing geometrical requirement for low nasal resistance and high exchange efficiency. Whereas resistance decreases with increasing gap width, the exchange efficiency is higher when the gap is thinner. The central result of this paper is the demonstration that the optimal geometry that balances these requirements has uniform gap width ℓ, which we predict in Eq. **7**. Strictly speaking, the optimal design of two parallel plates will not fit inside the head, but our calculations show that the bending and branching of the thin duct has only a modest effect on nasal efficiency. This suggests that the diverse morphology and labyrinth-like patterns of nasal cavities provide the lowest resistance for sufficient air conditioning under the geometric constraints imposed by the head. These physical and geometric constraints thus explain the large-scale morphology of nasal cavities, while the details likely exhibit additional constraints, like sufficient mechanical integrity and blood supply, which need to be studied in the future.

Our theory predicts that the surface area of the nasal cavity scales as $S \approx (VQ\mathcal{E})^{1/2}$, which implies the observed positive allometry (18, 22). This scaling explains why short-snouted

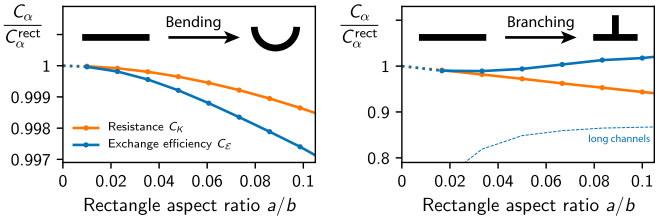

Fig. 5. Bending and branching does not affect the resistance K and scalar exchange efficiency $\mathcal{E}$ significantly. Shown are the prefactors C_K (orange) and $C_\mathcal{E}$ (blue) of (*Left*) bent and (*Right*) branched shapes normalized to the respective values for the corresponding rectangular shape with sides a and b as a function of its aspect ratio a/b. C_K follows from a numerical solution of Eq. **1**, while $C_\mathcal{E}$ has been calculated from Eq. **4** using the first 16 eigenmodes of Eq. **5** as described in *SI Appendix*. Parameters are given in Table 2, and the dashed blue line in *Right* shows $C_\mathcal{E}$ for channels that are elongated by a factor of 100, emphasizing the influence of the junction in longer channels.

animals (smaller V) have smaller surface area (29), and it quantifies the intuitive result that the nasal cavity can be smaller when heating and humidifying is less important (smaller $\mathcal{E}$). The latter might explain why birds have smaller nasal cavities compared with mammals of the same weight (5, 22), because their relatively longer tracheas could take over part of the air conditioning.

The scalar exchange efficiency $\mathcal{E}$ also depends on the tradeoff between conditioning the inhaled air and recapturing the heat and moisture during exhalation. When both processes are considered, a gradient in the boundary conditions along the nasal cavity is generally optimal, but the exact details depend on the environment and the physiological state of the animal. Here, it will be interesting to separate evolutionary adaptations, e.g., by related species living in different climates, from short-term adjustments caused by phenotypic plasticity, where, for instance, the gap width could be narrowed by swelling the epithelial tissue or secreting additional mucus. Our theory predicts how such changes affect the conditioning of inhaled air and the efficiency of expelling heat with exhaled air. It might also be used to study olfaction and the clearance of pollutants from inhaled air, which can both be described as passive scalar transport.

We also show that humans have surprisingly small nasal cavities with a reduced gap width and surface area compared with the expectations based on body mass. In fact, the volume of the human nasal cavity is almost 90% smaller than expected, which then requires a narrower gap to ensure adequate air conditioning. While a smaller nasal cavity likely evolved to accommodate a smaller face (5), the smaller gap width implies a larger resistance to airflow. To overcome this, the lungs could be made stronger, but this would require more energy. Instead, humans become obligate oral breathers during heavy physical activity, which also helps to dump heat (30). Because the oral cavity is much wider than the nasal cavity, its resistance and scalar exchange efficiency is lower. Consequently, heat can be dumped with the hotter exhaled air, but the inhaled air cannot be heated and humidified to the same extent as in the nasal cavity. It would thus be interesting to compare nasal and oral breathing in humans in more detail in the future.

ACKNOWLEDGMENTS. This research was funded by the National Science Foundation through Grant DMS-1715477 and Materials Research Science and Engineering Centers (MRSEC) Grant DMR-1420570, as well as by the Simons Foundation. D.Z. was also funded by the German Science Foundation through ZW 222/1-1.

1. Witmer LM (1995) Homology of facial structures in extant archosaurs (birds and crocodilians), with special reference to paranasal pneumaticity and nasal conchae. *J Morphol* 225:269–327.
2. Negus VE (1954) Introduction to the comparative anatomy of the nose and paranasal sinuses. *Ann R Coll Surg Engl* 15:141–171.
3. Macrini TE (2012) Comparative morphology of the internal nasal skeleton of adult marsupials based on x-ray computed tomography. *Bull Am Mus Nat Hist* 365: 1–91.
4. Maier W, Ruf I (2014) Morphology of the nasal capsule of primates—with special reference to Daubentonia and Homo. *Anat Rec* 297:1985–2006.
5. Lieberman D (2011) *The Evolution of the Human Head* (Harvard Univ Press, Cambridge, MA).
6. Quraishi M, Jones N, Mason J (1998) The rheology of nasal mucus: A review. *Clin Otolaryngol Allied Sci* 23:403–413.
7. Churchill SE, Shackelford LL, Georgi JN, Black MT (2004) Morphological variation and airflow dynamics in the human nose. *Am J Hum Biol* 16:625–638.
8. Clement PAR, Gordts F; Standardisation Committee on Objective Assessment of the Nasal Airway, IRS, and ERS (2005) Consensus report on acoustic rhinometry and rhinomanometry. *Rhinology* 43:169–179.
9. Bergman TL, Incropera FP (2011) *Introduction to Heat Transfer* (Wiley, New York).
10. Gates DM (2012) *Biophysical Ecology* (Courier, North Chelmsford, MA).
11. Sano M, Tamai K (2016) A universal transition to turbulence in channel flow. *Nat Phys* 12:249–253.
12. Eckhardt B, Schneider TM, Hof B, Westerweel J (2007) Turbulence transition in pipe flow. *Annu Rev Fluid Mech* 39:447–468.
13. Shi H, Kleinstreuer C, Zhang Z (2006) Laminar airflow and nanoparticle or vapor deposition in a human nasal cavity model. *J Biomech Eng* 128:697–706.
14. Craven BA, Paterson EG, Settles GS, Lawson MJ (2009) Development and verification of a high-fidelity computational fluid dynamics model of canine nasal airflow. *J Biomech Eng* 131:091002.
15. Zhao K, Dalton P, Yang GC, Scherer PW (2006) Numerical modeling of turbulent and laminar airflow and odorant transport during sniffing in the human and rat nose. *Chem Senses* 31:107–118.
16. Womersley JR (1955) Method for the calculation of velocity, rate of flow and viscous drag in arteries when the pressure gradient is known. *J Physiol* 127:553–563.
17. Squires TM, Messinger RJ, Manalis SR (2008) Making it stick: Convection, reaction and diffusion in surface-based biosensors. *Nat Biotechnol* 26:417–26.
18. Green PA, et al. (2012) Respiratory and olfactory turbinal size in canid and arctoid carnivorans. *J Anat* 221:609–621.
19. Tsilingiris P (2008) Thermophysical and transport properties of humid air at temperature range between 0 and 100 c. *Energy Convers Manage* 49:1098–1110.
20. Rouadi P, et al. (1999) A technique to measure the ability of the human nose to warm and humidify air. *J Appl Physiol* 87:400–406.
21. Cole P (1982) *The Nose: Upper Airway Physiology and the Atmospheric Environment* (Elsevier Biomed, Amsterdam), pp 163–189.
22. Owerkowicz T (2004) Respiratory innovations in monitor lizards, mammals and birds. PhD thesis (Harvard Univ, Cambridge, MA).
23. Liu Y, Johnson MR, Matida EA, Kherani S, Marsan J (2009) Creation of a standardized geometry of the human nasal cavity. *J Appl Phys* 106:784–795.
24. Shapira L, Shamir A, Cohen-Or D (2008) Consistent mesh partitioning and skeletonisation using the shape diameter function. *Vis Comput* 24:249–259.
25. Itō H (1969) Laminar flow in curved pipes. *J Appl Math Mech* 49:653–663.
26. Mori Y, Nakayama W (1967) Study on forced convective heat transfer in curved pipes (3rd report). *Int J Heat Mass Transf* 10:681–695.
27. Nishimura T, et al. (2016) Impaired air conditioning within the nasal cavity in flat-faced homo. *PLoS Comput Biol* 12:e1004807.
28. Schmid WD (1976) Temperature gradients in the nasal passage of some small mammals. *Comp Biochem Physiol A* 54:305–308.
29. van Valkenburgh B, et al. (2014) Respiratory and olfactory turbinals in feliform and caniform carnivorans: The influence of snout length. *Anat Rec* 297:2065–2079.
30. Bramble DM, Lieberman DE (2004) Endurance running and the evolution of homo. *Nature* 432:345–352.
31. Ms. Jeri Rodgers (2012) *Cavia porcellus*, Guinea Pig, Digital Morphology. Available at digimorph.org/specimens/Cavia_porcellus/. Accessed August 16, 2017.
32. Shah RK, London AL (1971) Laminar flow forced convection heat transfer and flow friction in straight and curved ducts–A summary of analytical solutions (Off Naval Res, Arlington, VA), Technical Report 75.
33. Stahl WR (1967) Scaling of respiratory variables in mammals. *J Appl Physiol* 22:453–460.
34. Herman IP (2016) *Physics of the Human Body* (Springer, New York).
35. Gilbert R, Auchincloss J, Brodsky J, Wa B (1972) Changes in tidal volume, frequency, and ventilation induced by their measurement. *J Appl Phys* 33:252–254.
36. Millar WJ (1986) Distribution of body weight and height: Comparison of estimates based on self-reported and observed measures. *J Epidemiol Community Health* 40:319–323.